Article

Magnetic Graphene Oxide Nanocomposites for Selective miRNA Separation and Recovery

Supapitch Uten,[○] Poramin Boonbanjong,[○] Yosaphon Prueksathaporn, Kiatnida Treerattrakoon, Nuankanya Sathirapongsasuti, Narong Chanlek, Supree Pinitsoontorn, Patraporn Luksirikul,* and Deanpen Japrung*

Read Online

ACCESS | Metrics & More | Article Recommendations | Supporting Information

Serum Circulating Biomarkers — Fe₃O₄@GO — miRNA Adsorption — Magnetic Separation — miRNA Recovery — Urea
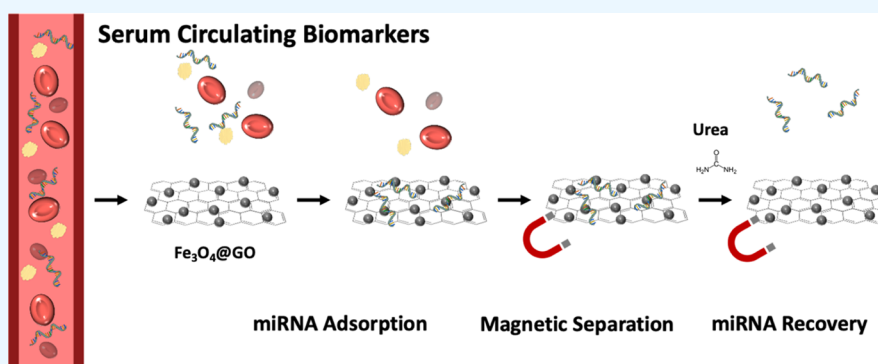
ABSTRACT: In this study, we developed magnetic graphene oxide composites by chemically attaching Fe_3O_4 nanoparticles to graphene oxide nanosheets. Characterization techniques, including Fourier transform infrared spectroscopy (FTIR), X-ray powder diffraction (XRD), Raman spectroscopy, thermogravimetric analysis (TGA), X-ray photoelectron spectroscopy (XPS), atomic force microscopy (AFM), and transmission electron microscopy (TEM), confirmed the successful synthesis of $Fe_3O_4@GO$ composites with desirable properties. The resulting composites exhibited superparamagnetic behavior, solubility, and compatibility for efficient miRNA separation. Using miR-29a as a model, we demonstrated the effective binding of miR-29a to the magnetic graphene oxide (GO) composites at an optimal concentration of 1.5 mg/mL, followed by a simple separation using magnetic forces. Additionally, the addition of 5.0 M urea enhanced the miRNA recovery. These findings highlight the potential use of our magnetic graphene oxide composites for the efficient separation and recovery of miR-29a, suggesting their broad applicability in various miRNA-based studies. Further exploration can focus on investigating endogenous miRNAs with aberrant expression patterns, contributing to the advancements in precision medicine.

INTRODUCTION

MicroRNAs (miRNAs) are small, single-stranded noncoding RNA molecules that play a critical role in physiological and pathological processes such as gene regulation and protein expression.[1] Recently, miRNAs have gained recognition as promising and reliable biomarkers for disease monitoring in clinical diagnosis, therapeutics, and prognosis. However, the clinical significance of miRNAs depends on the precise detection and isolation of miRNA biomarkers present in circulation.

To date, current technologies used for miRNA separation, including fluid-based methods such as guanidinium-acid-phenol extraction, glass fiber silica filter technology, and magnetic bead technology, have drawbacks in terms of low miRNA yield, compromised miRNA quality, use of toxic chemicals, and high costs.[2] To overcome these challenges, alternative methods for miRNA detection and isolation are

being explored. These strategies aim to improve the specificity and sensitivity of miRNA detection while offering a rapid and facile approach for miRNA separation using nanomaterials.

One promising nanomaterial for miRNA detection and isolation is graphene oxide (GO). GO is a two-dimensional (2D) structure with a hydrophobic basal plane and hydrophilic oxygenated functional groups. It exhibits excellent biocompatibility, a large surface area, and a strong affinity for adsorbing single-stranded nucleic acids (ssNAs) through $\pi-\pi$ interactions.[3−6] Additionally, GO can be modified by incorporating
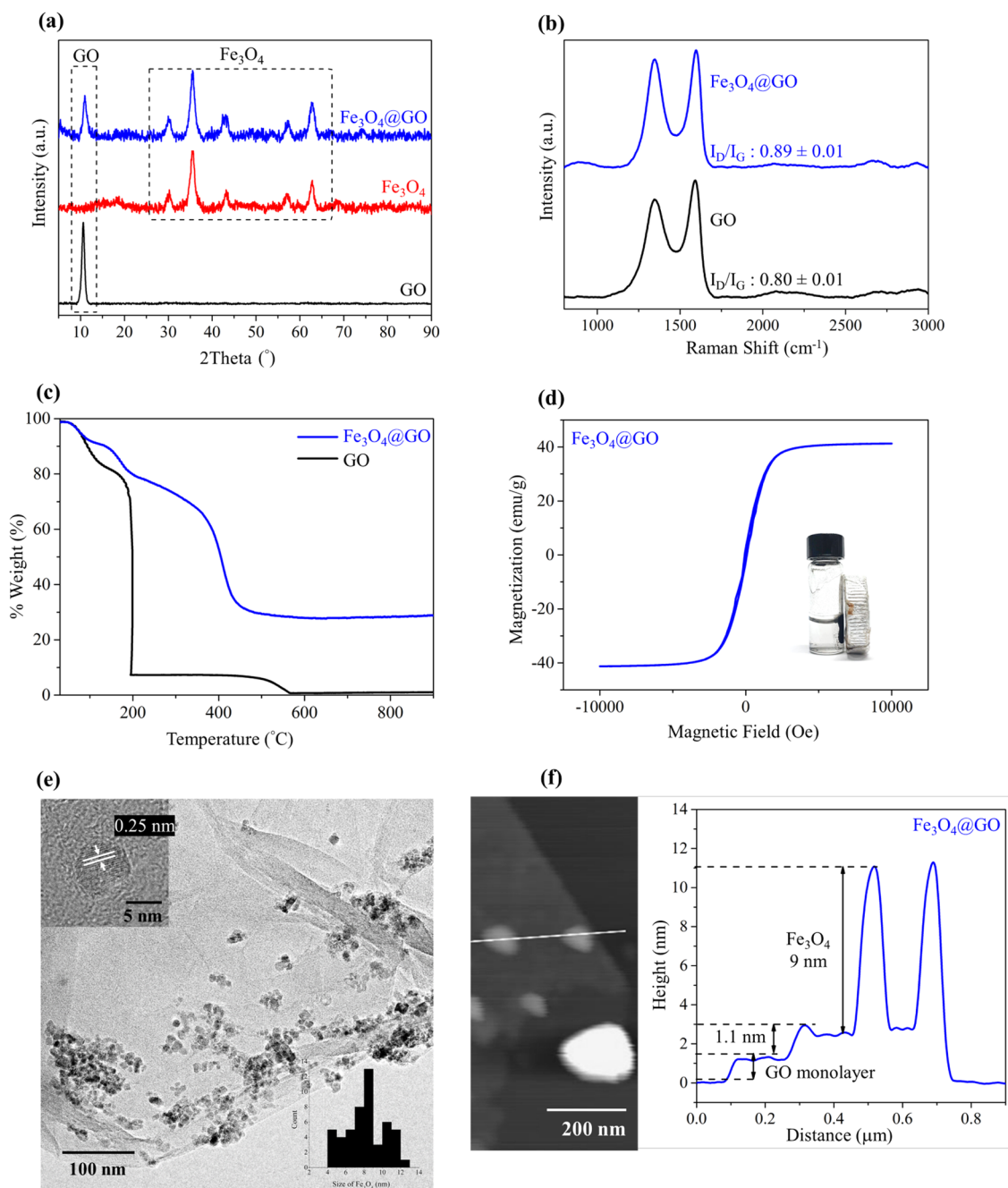
Figure 1. Characterization of graphene oxide (GO) and $Fe_3O_4@GO$ nanocomposite: (a) XRD spectra of GO, Fe_3O_4, and $Fe_3O_4@GO$, (b) Raman spectra comparing GO and $Fe_3O_4@GO$, (c) thermogravimetric analysis (TGA) curve comparing GO and $Fe_3O_4@GO$, (d) magnetization curve of $Fe_3O_4@GO$ with bottom inset showing the magnetic separation of $Fe_3O_4@GO$ in PBS, (e) TEM with HRTEM (inset) images of $Fe_3O_4@GO$, and (f) AFM micrograph with line scan across graphene oxide sheet to show the average thickness of GO layer and Fe_3O_4 decorated on GO sheet deposited on mica sheet,.

metal or metal oxide nanoparticles, utilizing epoxy, hydroxyl, and carboxyl groups.[7,8] This integration enabled the development of composite materials with enhanced functionalities.[9−16] In this study, we propose the use of magnetic graphene oxide nanomaterials ($Fe_3O_4@GO$) for rapid and facile miRNA separation. By attaching magnetic Fe_3O_4 nanoparticles to the GO structure, we created a GO-based magnetic extraction nanomaterial. This approach leverages the distinctive properties of GO and the magnetic characteristics of Fe_3O_4, offering a potential solution for the efficient isolation of miRNA from clinical samples.

■ RESULTS AND DISCUSSION

Characterizations of the As-Synthesized Fe_3O_4-Modified Graphene Oxide Nanocomposite. The preparation of Fe_3O_4-modified graphene oxide ($Fe_3O_4@GO$) nanocomposite was carried out through an amidation reaction of amino-Fe_3O_4 onto the GO nanosheet.[17] The success of the synthesized Fe_3O_4-modified graphene oxide ($Fe_3O_4@GO$) nanocomposite was confirmed using the combination of techniques, including X-ray powder diffraction (XRD), Raman spectroscopy (Raman), thermogravimetric analysis (TGA), atomic force microscopy (AFM), transmission

electron microscopy (TEM), Fourier transform infrared spectroscopy (FTIR), and X-ray photoelectron spectroscopy (XPS) (details of XPS and FTIR can be seen in the Supporting Information). First, the XRD patterns of Fe_3O_4@GO, graphene oxide (GO), and Fe_3O_4 were compared to identify the presence of Fe_3O_4 particles and the Fe_3O_4 nanoparticles onto the GO sheets. The obtained XRD spectra (Figure 1a) illustrate diffraction peaks at 2θ positions at 30.1, 35.5, 43.1, 57.0, and 62.7° corresponding to (220), (311), (400), (511), and (440) planes, respectively, which confirmed the Fe_3O_4 (magnetite) phase in our synthesized hybrid samples. Additionally, the average crystallite size of the Fe_3O_4 nanoparticles (approximately 8−9 nm) was derived from the Debye−Scherrer equation, which was in good agreement with results from TEM analysis (Figure 1e). Moreover, a peak located at 11.0° was observed, which corresponds to an interlayer distance (d) of 0.81 nm, indicating the presence of the (002) plane of graphene oxide in the composite sample. This suggests the presence of Fe_3O_4 nanoparticles onto the GO in our obtained Fe_3O_4@GO.

To gain a comprehensive understanding of the structural features of the synthesized Fe_3O_4-modified graphene oxide (Fe_3O_4@GO) nanocomposite, detailed analysis using transmission electron microscopy (TEM) was conducted. The transparency observed in the TEM image of the GO sheet (Figure S1a) indicated successful exfoliation of graphite oxide into few-layer GO sheets, which is consistent with the XRD results. In contrast, the TEM image of the Fe_3O_4 sample (Figure S1b) revealed the agglomeration of Fe_3O_4 nanoparticles, resulting in the formation of large clusters due to magnetic dipolar interactions among the magnetite nanoparticles. However, after modification, representative TEM images of the obtained hybrid Fe_3O_4@GO nanocomposite (Figure 1e) demonstrated narrow particle sizes with a high dispersion of Fe_3O_4 nanoparticles uniformly deposited on the GO sheets. The observed particle size of Fe_3O_4 nanoparticles was determined to be 8.9 ± 0.9 nm, which corresponds well with the size calculated from the XRD analysis (Figure 1e, inset). Furthermore, the lattice fringes with a d-spacing of 0.25 nm agreed well with the (311) planes of Fe_3O_4, which is confirmed by the HRTEM image (Figure 1e, inset). Thus, these TEM findings provide visual confirmation of the successful synthesis and structural characteristics of the Fe_3O_4 deposited on the GO sheet in the Fe_3O_4@GO nanocomposite sample.

Atomic force microscopy (AFM) was then carried out to receive the information on variant thickness of the GO sheet and Fe_3O_4@GO composite. GO thickness was determined by yielding a measurement of approximately 1.1 nm, as depicted in Figure S1c, which is similar to the thickness of a single layer of GO. Furthermore, for the Fe_3O_4@GO composite, the thickness of the GO sheet increases to 11.0 nm, as illustrated in Figure 1f. This different thickness is reminiscent of the presence of a graphene monolayer along with the theoretical length of the modified amino-Fe_3O_4 and the carboxamide linkage. The AFM results provide additional confirmation for the characterization of the Fe_3O_4@GO nanocomposite with Fe_3O_4 nanoparticles of size 8−9 nm attached to the GO surface, which is identical to the XRD and TEM results.

Hence, Raman spectroscopy was employed to analyze the chemical modifications of the hybrid Fe_3O_4@GO samples. Figure 1b displays the Raman spectrum of GO, exhibiting two distinct peaks at 1360 and 1583 cm^{-1}, corresponding to the D and G bands, respectively. The D band is typically associated with the disorder in GO arising from defects related to vacancies, grain boundaries, and amorphous carbon species. On the other hand, the G band is attributed to the presence of sp^2 carbon domains in the basal plane. The relative ratio of D band to G band (I_D/I_G) is commonly used to assess the graphitization degree and any change in carbon atom environment that affects the periodicity of the carbon structure such as defects resulting from the incorporation of disorders and chemicals added.[19,20] An increase in the intensity of the D and G ratio depends on a density of defects or disorder in the carbon lattice. The ratio of I_D/I_G is determined by dividing the intensity of D by the intensity of G in which each mode is normalized by setting the maximum intensity. Upon the synthesis of the Fe_3O_4@GO composite, the two peaks are present at 1352 and 1582 cm^{-1}, which can be assigned to D and G in the obtained graphene oxide composite, indicative of sp^3-hybridized carbon and sp^2-hybridized bond in the structure of GO composite, respectively. After modification, an increase of the relative I_D/I_G intensity ratio from 0.80 ± 0.01 for GO to 0.89 ± 0.01 for the Fe_3O_4@GO composite is observed. These observations suggest a significant increase in defects on the GO sheet due to the attachment of Fe_3O_4 indicating the change in structural hybridization on the graphene-based nanocomposite.

The thermal stability and functionalization of the Fe_3O_4@GO composites were examined by thermogravimetric analysis (TGA), as it has been previously demonstrated that heating functionalized graphene oxide (GO) can lead to the removal of organic functionalities through oxidation reactions. In this study, TGA treatment was performed on both GO and Fe_3O_4@GO composites. Figure 1c illustrates the TGA curves of the Fe_3O_4@GO composites in comparison to those of the precursor GO nanosheet. The initial weight loss observed at 120 °C can be attributed to the evaporation of adsorbed water and labile oxygenated functional groups present in the GO structures. Notably, the TGA curve of GO exhibits a significant weight loss starting at approximately 190 °C, indicating the elimination of oxygenated functional groups such as hydroxyl, epoxy, and carboxylate. The result suggests that GO exhibits thermal instability under an air atmosphere. In contrast, the Fe_3O_4@GO composites display two-step weight losses occurring at around 120−300 and 300−600 °C. The weight losses can be attributed to the removal of oxygenated or organic functional groups as well as the combustion of the carbon skeletal structure. The final residual weight observed at 600 °C for the Fe_3O_4@GO composites was approximately 29.14%, which can be attributed to the presence of Fe_3O_4 nanoparticles adsorbed within the layers among the GO sheets which is related to the content of 30% Fe_3O_4 in Fe_3O_4@GO composite. These results are also consistent with the presence of organic functional groups observed by FTIR spectroscopy (Figure S2), where characteristic bands of the oxygenated functional moieties on GO and Fe_3O_4@GO composite and the carboxamide bond confirmed the existence of chemical bonding. Overall, the TGA results provide evidence of the thermal stability and functionalization of the Fe_3O_4@GO composites, further supporting the successful synthesis and characteristics of the nanocomposite.

The magnetic properties of the Fe_3O_4@GO composites were assessed by using the vibrational sample magnetometer (VSM) technique at room temperature. Figure 1d illustrates the magnetization hysteresis loop, which exhibits an S-like shape. It indicates that the Fe_3O_4@GO composites exhibit
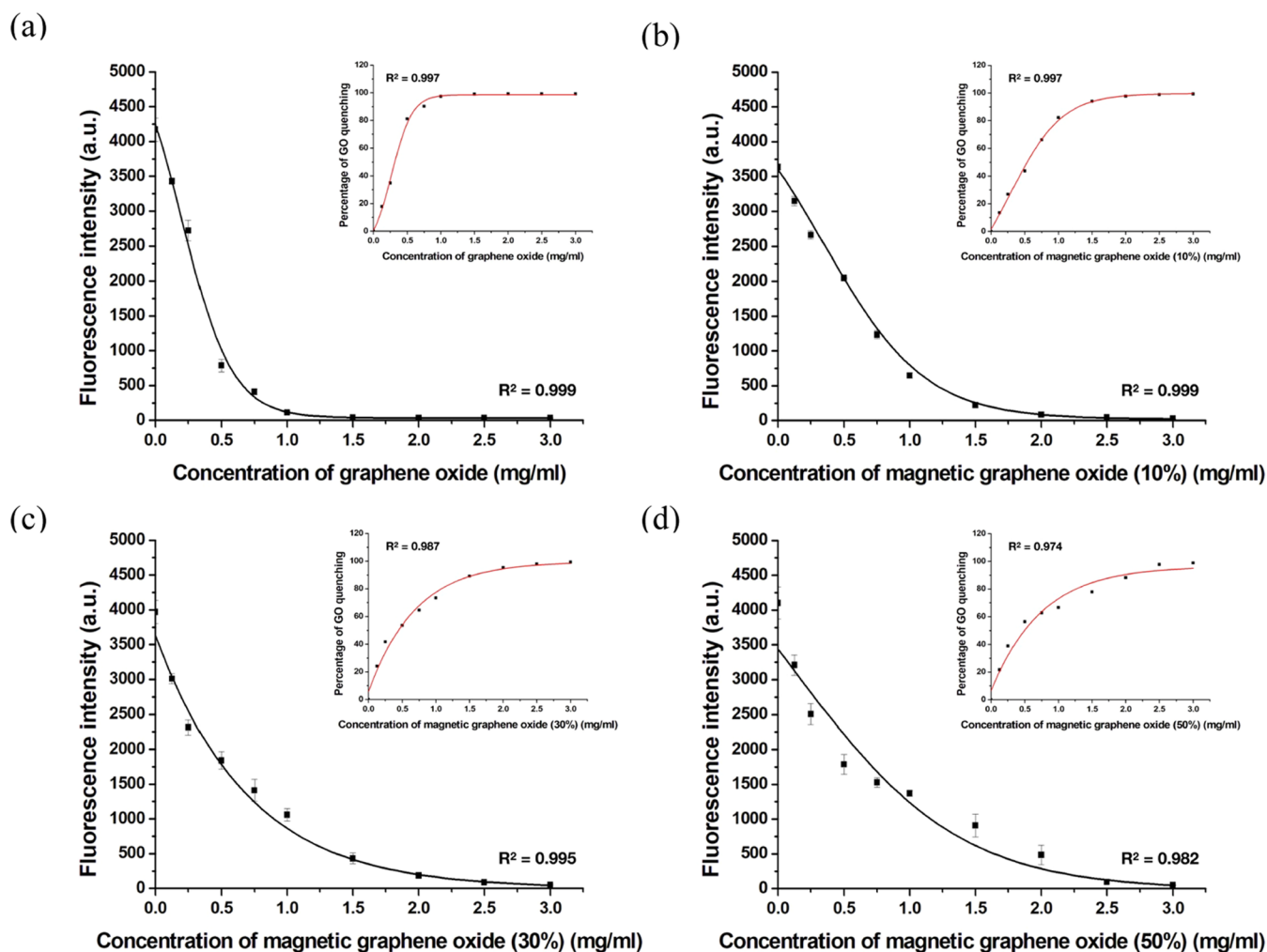
Figure 2. Effects of magnetic graphene oxide concentration on the fluorescence intensity of Cy5-labeled probes (Cy5-miR-29a). The fluorescence intensity of Cy5-miR-29a was measured in the presence of different concentrations of graphene oxide or magnetic graphene oxide, with concentrations ranging from 0 to 3 mg/mL. The magnetic graphene oxide samples included (a) no magnetic, (b) 10% magnetic, (c) 30% magnetic, and (d) 50% magnetic.

nearly zero magnetic coercivity, which confirms the superparamagnetic behavior of the synthesized $Fe_3O_4@GO$ composites. The saturation magnetization of the obtained $Fe_3O_4@GO$ was measured to be approximately 40.4 emu g^{-1}. Furthermore, as shown in the inset of Figure 1d, the $Fe_3O_4@GO$ composites can be easily collected using a magnet, as evidenced by their attraction to the magnet when placed in close proximity. This observation highlights the magnetic responsiveness of the $Fe_3O_4@GO$ composites, suggesting their potential convenience for miRNA isolation applications. It can be noted that the $Fe_3O_4@GO$ composites which exhibited superparamagnetic properties would be a favorable candidate for efficient and effective miRNA separation processes.

Optimization of $Fe_3O_4@GO$ Concentration for Efficient Fluorescence Quenching Properties. To determine the most effective concentration and magnetic percentage of the $Fe_3O_4@GO$ nanocomposite for miRNA isolation, we performed a fluorescence-quenching-based assay utilizing Cy5-labeled miR-29a. Different concentrations of $Fe_3O_4@GO$, varying in magnetic percentages, were examined to assess the fluorescence intensity of 1 μM Cy5-labeled miR-29a. The range of $Fe_3O_4@GO$ concentrations investigated spanned from 0 to 3 mg/mL.

As the amount of $Fe_3O_4@GO$ increased, the fluorescence intensity of the Cy5-labeled miR-29a decreased, following a pattern consistent with a Sigmoidal Boltzmann fitting, as shown in Figure 2. The close fit to this curve, with an R^2 value greater than 0.98, shows that the miRNA is successfully attaching to the GO. The quenching of GO is attributed to energy transfer from the fluorophore to the $\pi-\pi$ system of GO. Notably, the fluorescence signal diminished by more than 80% when at least 1.5 mg/mL $Fe_3O_4@GO$, with different magnetic percentages, was introduced. This outcome confirms the effective quenching capability of the nanocomposite. Based on these findings, we determined that the optimal concentration of $Fe_3O_4@GO$ for miRNA isolation is 1.5 mg/mL, with a magnetic percentage of 30%. Subsequently, this concentration was employed in subsequent experiments to ensure an ideal combination of quenching properties and solubility for the $Fe_3O_4@GO$ nanocomposite.

Determining the Optimal Urea Concentration for miR-29a Recovery and Method Validation. The investigation focused on the effect of urea on the $Fe_3O_4@GO$ complex to determine the optimal concentration for miRNA recovery experiments. The concentration of urea was varied from 0.5 to 8.0 M, and the results demonstrated that a final

Fe₃O₄@GO preparation
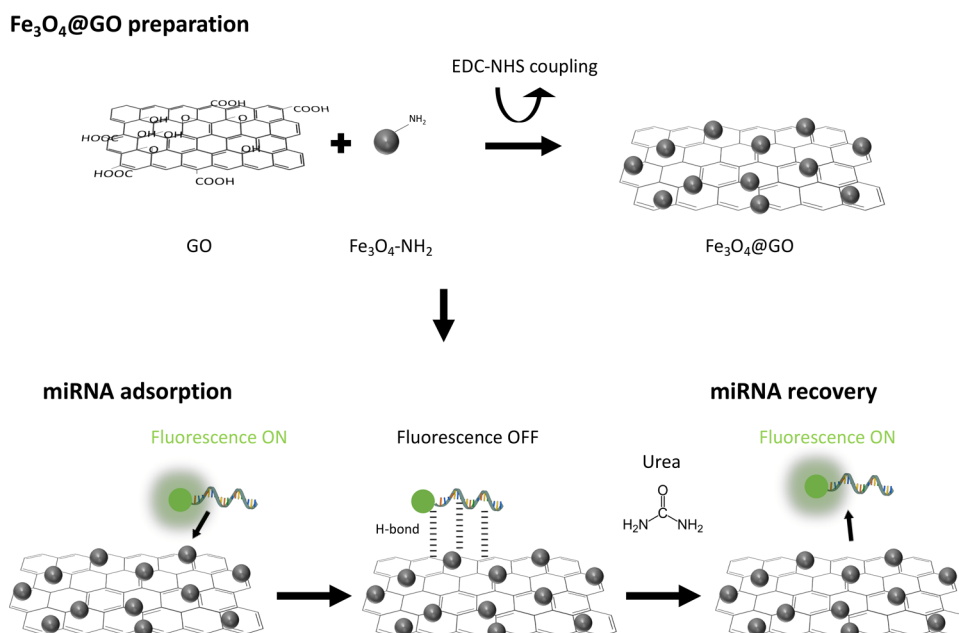
Figure 3. Preparation of magnetic graphene oxide and its application in conjunction with urea for miRNA separation and recovery. The top panel illustrates the preparation of the magnetic graphene oxide nanocomposite, while the bottom panel demonstrates the separation and recovery processes. Fluorescent-labeled miRNA is adsorbed onto the magnetic graphene oxide sheets, causing fluorescence quenching. The recovery process is initiated by the addition of urea, which disrupts the bond between graphene oxide and miRNA. This results in the detachment of the miRNA and the subsequent restoration of the fluorescence signal.
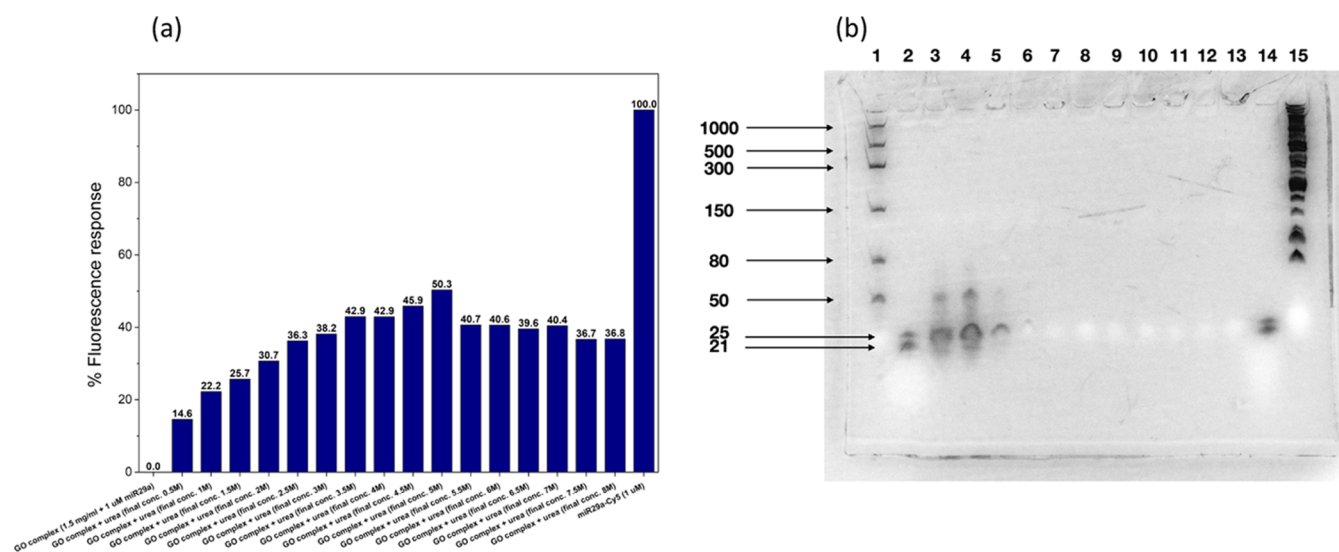
Figure 4. Impact of urea on miRNA recovery. (a) Changes in fluorescence intensity before and after the addition of various concentrations of urea. (b) Urea-PAGE (5%) gel images displaying recovered miR-29a. Lanes 1 and 15 indicate the low-range ssRNA ladder and 100 bp ladder, respectively. Lanes 2 and 14 represent the microRNA ladder. Lane 3 serves as the positive control containing miR-29a. Lanes 4 to 12 exhibit recovered miR-29a at different concentrations: 100 μM, 10 μM, 1 μM, 100 nM, 10 nM, 1 nM, 100 pM, 10 pM, and 1 pM, respectively. Lastly, lane 13 functions as the negative control, featuring recovered magnetic graphene oxide.

concentration of 5.0 M urea yielded the highest fluorescence intensity. This concentration was selected for further experiment due to its effectiveness. It is known that GO binds to miRNA through hydrogen bonding or $\pi-\pi$ interactions with miRNA nucleobases, supported by previous reports suggesting the presence of hydrogen bonds between the hydroxyl/carboxyl group of GO and the amine/carbonyl group of the nucleobase.[5] This ability of urea to denature nucleic acids through extensive hydrogen bonding with amino acid residues and nucleobases explains its effectiveness in separating GO and

miRNA. Figure 3 depicts a schematic for miRNA separation and recovery using magnetic graphene oxide and urea.

miRNA recovery experiments aimed to demonstrate the binding of miRNA by Fe₃O₄@GO at different concentrations and the capability of urea to separate miRNA from Fe₃O₄@GO at various concentrations. The results from two main experiments conducted before and after the addition of urea, as shown in Figure 4, revealed significant findings. Fe₃O₄@GO at a concentration of 1.0 mg/mL effectively bound miRNA at different concentrations, with clear fluorescence intensity

observed at 1.0 μM miR-29a-Cy5. Comparing the results of miR-29a-Cy5 at 1.0 μM, the fluorescence intensity reached approximately 590 au when the external magnetic field was applied to separate miRNA before adding urea. However, after the addition of urea and the application of an external magnetic field, the fluorescence intensity increased to approximately 1125 au. This significant enhancement in fluorescence intensity indicated the improved recovery of miRNA following the addition of urea. It is important to note that at low concentrations of miR-29a-Cy5, the fluorescence intensity was relatively low, possibly due to the limited amount of miRNA present.

These results clearly established 5.0 M as the optimal concentration of urea for miRNA recovery experiments as it yielded the highest fluorescence intensity. Moreover, the study successfully demonstrated the binding capability of $Fe_3O_4@$ GO and its effective separation of miRNA from the complex using urea. The recovery of miR-29a was further confirmed through an analysis of a polyacrylamide gel with 8 M urea. Overall, these findings solidify the efficacy of the proposed method in miRNA recovery and offer valuable insights for future applications in miRNA-related studies.

Validation of a Magnetic Graphene Oxide-Based Method for Spike-in miRNA Recovery from Serum Using TaqMan qRT-PCR. Validation of the proposed method involved the utilization of TaqMan qRT-PCR, a highly sensitive and quantitative technique widely employed in miRNA analysis. By specifically targeting miR-29a, which has implications in various biological contexts and diseases, the study aimed to assess the efficiency of the proposed method in recovering spike-in miRNAs from serum samples. The TaqMan qRT-PCR analysis revealed the detectability of miR-29a in the extracted spike-in miRNAs from human serum. Notably, the inclusion of miRNA concentrations ranging from 10 ng to 10 μg enabled a comprehensive evaluation of the method's efficacy across a broad range of miRNA levels. The consistent observation of Ct values below 35 for all tested concentrations indicated successful miRNA recovery, with lower Ct values indicative of higher miRNA levels (Figure 5).

These findings provide robust evidence supporting the potential of the magnetic graphene oxide-based miRNA
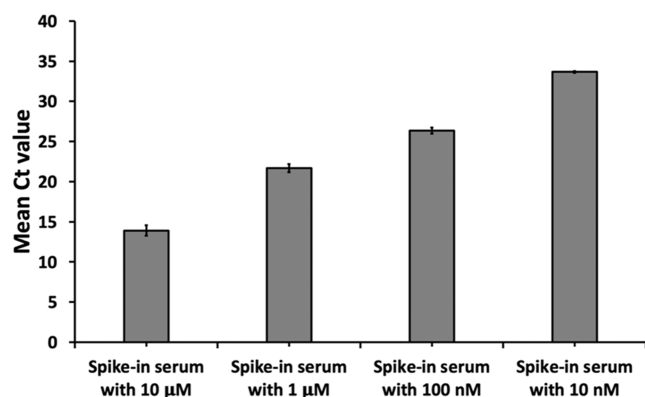
Figure 5. Quantification of recovered miR-29a from spike-in serum. The expression levels of recovered miR-29a were determined using qRT-PCR, with lower Ct values indicating higher miRNA expression. Error bars represent the estimated variation based on duplicate experiments.

extraction approach for retrieving miRNAs with abnormal expression levels from diverse body fluids. The ability to detect miR-29a, a specific miRNA of interest, highlights the method's specificity and sensitivity in isolating target miRNAs. Such capabilities pave the way for further exploration of miRNAs as potential biomarkers for disease diagnosis, prognosis, and monitoring. Moreover, the validated method's applicability extends beyond spike-in miRNAs, offering opportunities to investigate endogenous miRNAs with aberrant expression patterns in various body fluids. By leveraging the magnetic properties of graphene oxide and its affinity for miRNAs, this approach holds great promise in advancing noninvasive miRNA-based diagnostic strategies, ultimately contributing to the field of precision medicine.

It is crucial to underscore the unique advantages of utilizing $Fe_3O_4@GO$ for miRNA separation and extraction, particularly when contrasted with other nanomaterials (refer to Table S1). The superparamagnetic properties of $Fe_3O_4@GO$ enable a rapid and straightforward separation process without the necessity for centrifugation, presenting a marked advantage over the various existing methods and materials. This is especially advantageous for potential applications in high-throughput and real-time settings, where rapidity and efficacy are paramount. Additionally, the composites' ability to effectively bind and separate miRNA at optimized concentrations highlights its utility and potential in progressing miRNA-based diagnostic approaches, especially for miRNAs exhibiting abnormal expression levels.

CONCLUSIONS

In conclusion, the synthesized Fe_3O_4-modified graphene oxide ($Fe_3O_4@GO$) nanocomposite demonstrated favorable properties, particularly the successful attachment of Fe_3O_4 nanoparticles onto GO sheets and optimized concentrations of $Fe_3O_4@GO$ and urea for efficient miRNA recovery, showcasing effective miRNA binding and separation. Validated using TaqMan qRT-PCR, the method confirmed the detectability of miR-29a in spiked-in miRNAs from human serum across a wide dynamic range. Significantly, the innovative incorporation of urea, a nontoxic chaotropic agent, ensures enhanced miRNA recovery by disrupting hydrophobic interactions, presenting a notable advancement, especially considering the safety and efficiency of the method in clinical settings. This methodology, which adeptly combines the magnetic separation capabilities of $Fe_3O_4@GO$ with the miRNA recovery-enhancing properties of urea, stands out particularly for potential applications in high-throughput and real-time settings, where rapid, efficient, and safe miRNA extraction methods are crucial. The findings illuminate the potential of the magnetic graphene oxide-based approach for retrieving miRNAs with abnormal expression levels, thereby paving the way for noninvasive miRNA-based diagnostics in various diseases and further exploration into endogenous miRNAs with aberrant expression patterns, advancing the field of precision medicine.

METHODS

Synthesis of Fe_3O_4-Modified Graphene Oxide Nanocomposite. Graphene oxide (GO) was synthesized using the modified Hummers and Offeman method.[18] Magnetic particles were prepared through the coprecipitation of Fe^{2+} and Fe^{3+} in an aqueous solution. To obtain amine-functionalized magnetic particles ($Fe_3O_4-NH_2$), the magnetic particles were further
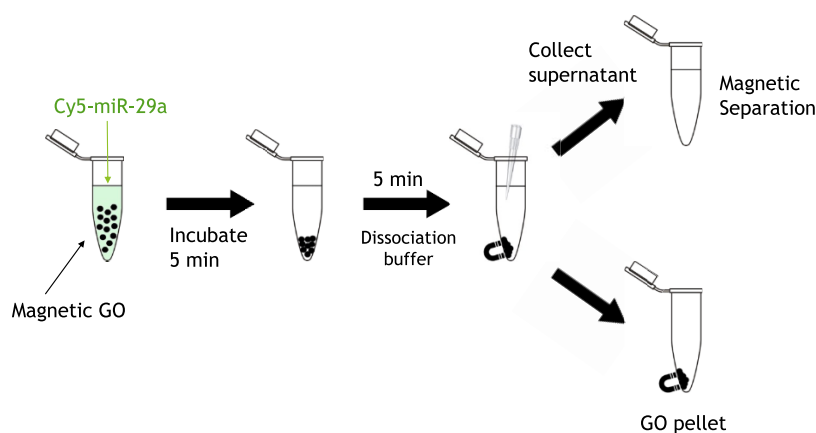
Figure 6. miRNA isolation using magnetic graphene oxide. The process involves the formation of an miRNA-magnetic graphene oxide complex by incubating the magnetic graphene oxide with synthetic miR-29a oligonucleotides for 5 min. Subsequently, the complex is dissociated using a dissociation buffer containing urea, followed by the separation of magnetic graphene oxide using a magnet.

modified with 3-aminopropyltriethoxysilane (APTES).[17] In the amidation process, the carboxylic groups in GO were coupled with the amino groups of the magnetic particles using EDC-NHS coupling agents.[17] To initiate the synthesis, $Fe_3O_4-NH_2$ and GO were added to 160 mL of DI water and sonicated for 30 min. Subsequently, 22.8 μL of EDC and 16 mg of NHS were added to the solution, which was then stirred at 80 °C for 24 h. After completion of the reaction, the solution was subjected to magnetic separation, followed by three washes with DI water. Finally, the obtained Fe_3O_4@GO nanocomposite was dried and stored at room temperature.

Optimization of Fe_3O_4−Modified Graphene Oxide Concentration for Fluorescence Quenching. To optimize the concentration of magnetic graphene oxide, we evaluated its ability to quench the fluorescence signal. A magnetic graphene oxide solution was prepared by dissolving 5 mg of 30% magnetic graphene oxide powder in 1 mL of sterile water, followed by 20 min of sonication until homogeneity was achieved. Subsequently, 10 μL of various concentrations of magnetic graphene oxide (ranging from 0 to 3 mg/mL) were mixed with 10 μL of 1 μM Cy5-labeled miR-29a and incubated at room temperature for 5 min in the dark. The volume was then adjusted to 200 μL. Finally, the fluorescence intensity was measured using a Quantus portable fluorometer (Promega Corp., Madison, WI) with an excitation at 630 nm and emission at 670 nm.

Serum Preparation and Collection. To prepare the serum samples, 10 blood samples were collected from Ramathibodi Hospital, Mahidol University, Bangkok, Thailand (Ethical approval no. COA. MURA2014/369). Peripheral blood (10 mL) was obtained from the median cubital vein. The blood samples were collected into red-topped tubes without an anticoagulant (Vacuette, LabNet International, Inc., Edison, New Jersey). Subsequently, the tubes were centrifuged at 5000g for 10 min in a refrigerated centrifuge to obtain clear supernatant serum. The obtained serum samples were aliquoted and stored at −80 °C until further use.

Gel Electrophoresis and Visualization. For gel electrophoresis, a urea-denaturing 5% polyacrylamide gel (Urea-PAGE) was prepared using a mixture of 40% acrylamide/bis solution (29:1), 10× TBE, 8 M urea, TEMED, and 30% ammonium persulfate following the standard protocol. The sample was mixed with RNA loading dye in a 1:1 ratio to achieve a final volume of 20 μL. The mixture was heated at 65

°C for 5 min and immediately cooled on ice for 5 min. All samples, along with the low-range RNA ladder, DNA ladder, and miRNA ladder, were loaded onto the 5% Urea-PAGE gel. Gel electrophoresis was performed in 1× TBE buffer under a constant voltage of 200 V for 30 min. Following electrophoresis, the gels were stained with 1× SYBR Gold Nucleic Acid Gel stain, following the manufacturer's protocol, and visualized using an in vivo imaging system (in vivo FX PRO, Bruker, Germany).

Evaluating the Efficiency of Fe_3O_4-Modified Graphene Oxide for miRNA Separation and Recovery. To demonstrate the efficacy of magnetic graphene oxide for miRNA isolation, different concentrations of synthetic miR-29a oligonucleotides were utilized, including 100, 10, 1 μM, 100, 10, 1 nM, 100, 10, and 1 pM. A 30% magnetic graphene oxide solution (1.5 mg/mL) was mixed with the various concentrations of miR-29a at a ratio of 2:1 and incubated at room temperature for 5 min to form the miRNA-magnetic graphene oxide complex. Subsequently, the complex was dissociated using a dissociation buffer, followed by the separation of magnetic graphene oxide using a magnet (Figure 6). The concentrations of isolated miRNA were measured using a NanoDrop One/OneC Microvolume ultraviolet−visible (UV−vis) spectrophotometer (Thermo Fisher Scientific, Waltham, MA). Additionally, the isolated miRNA samples were analyzed by using a 5% polyacrylamide gel with 8 M urea (Urea-PAGE gel) for further validation and visualization of the miRNA isolation.

Evaluating the Efficiency of Fe_3O_4-Modified Graphene Oxide for miRNA Isolation from Spiked-In Human Serum. To validate the efficiency of magnetic graphene oxide for miRNA isolation from clinical samples, different concentrations of synthetic miR-29a oligonucleotides (Table 1) were spiked into pooled human serum and isolated using the proposed method. The 30% magnetic graphene oxide solution (1.5 mg/mL) was mixed with the various concen-

Table 1. Sequences of Oligonucleotides and Probes Used in This Study

oligonucleotides	sequence (5′ → 3′)
miR-29a	UAG CAC CAU CUG AAA UCG GUU A
Tag/Cy5-miR-29a	Cy5-GAT TTC AGA TGG

trations of miR-29a at a ratio of 2:1 and incubated at room temperature for 5 min to form the miRNA-magnetic graphene oxide complex. Subsequently, the complex was washed with a wash buffer (60 mM sodium acetate, 10 mM Tris-HCl, 60% (v/v) ethanol) and then dissociated using a dissociation buffer (5 M urea in 1XPBS buffer).

The concentrations of isolated miRNA were measured using a NanoDrop One/OneC Microvolume UV−vis spectrophotometer (Thermo Fisher Scientific, Waltham, MA). Furthermore, the isolated miRNA samples were analyzed by using a 5% polyacrylamide gel with 8 M urea (Urea-PAGE gel) for further validation and visualization. This study demonstrates the capability of magnetic graphene oxide for efficient miRNA isolation from spiked human serum samples.

Quantification of Isolated miR-29a Using TaqMan qRT-PCR. To quantify the isolated miR-29a, the recovered miR-29a from the spike-in experiment was reverse-transcribed into cDNA using the TaqMan Advanced miRNA cDNA Synthesis kit (Applied Biosystems) following the manufacturer's instructions. The levels of isolated miR-29a were analyzed by using quantitative real-time PCR (qRT-PCR). In brief, the qRT-PCR reaction was performed in a 20 μL reaction volume, including 10 μL of 2× TaqMan Fast Advanced Master mix, 1 μL of 20× TaqMan Advanced miRNA assay, 4 μL of nuclease-free water, and 5 μL of cDNA (diluted 1:50), using a CFX96 Touch Real-Time PCR Detection System (BIO-RAD) according to the manufacturer's instructions. The thermal cycling conditions were as follows: 95 °C for 20 s, followed by 40 cycles of 95 °C for 3 s and 60 °C for 30 s. This analysis employed TaqMan qRT-PCR to accurately quantify the levels of isolated miR-29a in the samples obtained during the isolation process.

◼ ASSOCIATED CONTENT

Ⓢ Supporting Information

The Supporting Information is available free of charge at https://pubs.acs.org/doi/10.1021/acsomega.3c05919.

> Microscopic characterization and particle size distribution analysis, transmission electron microscopy image (Figure S1); FTIR spectra of three materials: graphene oxide (GO), amino-functionalized Fe_3O_4 nanoparticles ($Fe_3O_4-NH_2$), and the composite $Fe_3O_4@GO$, TEM images of graphene oxide (GO), Fe_3O_4 nanoparticles, and atomic force microscopy (AFM) images of GO (Figure S2); XPS spectra of the Fe_3O_4, $Fe_3O_4-NH_2$, GO, and $Fe_3O_4@GO$, high-resolution XPS spectrum in the N 1s peak region of $Fe_3O_4-NH_2$, high-resolution XPS spectra in the C 1s peak region of GO and $Fe_3O_4@$ GO, high-resolution XPS spectra in the Fe2p peaks region of Fe_3O_4, $Fe_3O_4-NH_2$, and $Fe_3O_4@GO$ (Figure S3); and comparative analysis of $Fe_3O_4@GO$ with other nanomaterials for miRNA separation and extraction (Table S1) (PDF)

◼ AUTHOR INFORMATION

Corresponding Authors

Patraporn Luksirikul − *Department of Chemistry, Faculty of Science, Kasetsart University, Bangkok 10900, Thailand; Research Network NANOTEC-KU on Nanocatalysts and Nanomaterials for Sustainable Energy and Environment, Kasetsart University, Bangkok 10900, Thailand;* Email: fscipplu@ku.ac.th

Deanpen Japrung − *National Nanotechnology Center (NANOTEC), National Science and Technology Development Agency (NSTDA), Pathumthani 12120, Thailand;* ⓞ orcid.org/0000-0003-4206-6641; Email: deanpen@nanotec.or.th

Authors

Supapitch Uten − *Department of Chemistry, Faculty of Science, Kasetsart University, Bangkok 10900, Thailand*

Poramin Boonbanjong − *Program in Translational Medicine, Faculty of Medicine Ramathibodi Hospital, Mahidol University, Bangkok 10400, Thailand;* ⓞ orcid.org/0000-0003-2703-1176

Yosaphon Prueksathaporn − *National Nanotechnology Center (NANOTEC), National Science and Technology Development Agency (NSTDA), Pathumthani 12120, Thailand*

Kiatnida Treerattrakoon − *National Nanotechnology Center (NANOTEC), National Science and Technology Development Agency (NSTDA), Pathumthani 12120, Thailand; Department of Pure and Applied Chemistry, Technology and Innovation Centre, University of Strathclyde, Glasgow G1 1RD, United Kingdom*

Nuankanya Sathirapongsasuti − *Program in Translational Medicine, Faculty of Medicine Ramathibodi Hospital, Mahidol University, Bangkok 10400, Thailand*

Narong Chanlek − *Synchrotron Light Research Institute (Public Organization), Nakhon Ratchasrima 30000, Thailand*

Supree Pinitsoontorn − *Institute of Nanomaterials Research and Innovation for Energy (IN-RIE), Khon Kaen University, Khon Kaen 40002, Thailand;* ⓞ orcid.org/0000-0002-4921-1541

Complete contact information is available at:
https://pubs.acs.org/10.1021/acsomega.3c05919

Author Contributions

ᴼS.U. and P.B. contributed equally to this work. The manuscript was written through contributions of all authors. All authors have given approval to the final version of the manuscript.

Notes

The authors declare no competing financial interest.

ABBREVIATIONS

miRNAs, microRNAs; Fe$_3$O$_4$@GO, magnetic graphene oxide nanomaterials; XRD, X-ray diffraction analysis; TEM, transmission electron microscopy; FTIR, Fourier transform infrared analysis; TGA, thermogravimetric analysis; VSM, vibrating-sample magnetometer technique; XPS, X-ray photoelectron spectroscopy

REFERENCES

(1) Gao, Y.; Lin, L.; Li, T.; Yang, J.; Wei, Y. The role of miRNA-223 in cancer: Function, diagnosis and therapy. *Gene* **2017**, *616*, 1−7.

(2) Johnson, M. Kits for RNA Extraction, Isolation, and Purification. *Mater. Methods* **2012**, *2*, No. 201, DOI: 10.13070/mm.en.2.201.

(3) Wang, Y.; Li, Z.; Wang, J.; Wang, J.; Li, J.; Lin, Y. Graphene and graphene oxide: biofunctionalization and applications in biotechnology. *Trends Biotechnol.* **2011**, *29* (5), 205−212.

(4) Chung, C.; Kim, Y.-K.; Shin, D.; Ryoo, S. R.; Hong, B. H.; Min, D.-H. Biomedical Applications of Graphene and Graphene Oxide. *Acc. Chem. Res.* **2013**, *46* (10), 2211−2224, DOI: 10.1021/ar300159f.

(5) Huang, P.-J.; Liu, J. Separation of Short Single- and Double-Stranded DNA Based on Their Adsorption Kinetics Difference on Graphene Oxide. *Nanomaterials* **2013**, *3*, 221−228.

(6) Park, J. S.; Na, H.-K.; Min, D.-H.; Kim, D.-E. Desorption of single-stranded nucleic acids from graphene oxide by disruption of hydrogen bonding. *Analyst* **2013**, *138* (6), 1745−1749.

(7) Georgakilas, V.; Otyepka, M.; Bourlinos, A. B.; Chandra, V.; Kim, N.; Kemp, K. C.; Hobza, P.; Zboril, R.; Kim, K. S. Functionalization of Graphene: Covalent and Non-CovalentApproaches, Derivatives and Applications. *Chem. Rev.* **2012**, *112*, 6156−6214, DOI: 10.1021/cr3000412.

(8) Fan, K.; Yang, R.; Zhao, Y.; Zang, C.; Miao, X.; Qu, B. H.; Lu, L. A fluorescent aptasensor for sensitive detection of isocarbophos based on AT-rich three-way junctions DNA templated copper nanoparticles and Fe$_3$O$_4$@GO. *Sens. Actuators, B* **2020**, *321*, No. 128515.

(9) Yan, H.; Xu, Y.; Lu, Y.; Xing, W. Reduced Graphene Oxide-Based Solid-Phase Extraction for the Enrichment and Detection of microRNA. *Anal. Chem.* **2017**, *89* (19), 10137−10140.

(10) Pakapongpan, S.; Tuantranont, A.; Poo-arporn, R. P. Magnetic Nanoparticle-Reduced Graphene Oxide Nanocomposite as a Novel Bioelectrode for Mediatorless-Membraneless Glucose Enzymatic Biofuel Cells. *Sci. Rep.* **2017**, *7* (1), No. 12882.

(11) Zhang, Y.; Chen, B.; Zhang, L.; Huang, J.; Chen, F.; Yang, Z.; Yao, J.; Zhang, Z. Controlled assembly of Fe$_3$O$_4$ magnetic nanoparticles on graphene oxide. *Nanoscale* **2011**, *3* (4), 1446−1450.

(12) Pervez, Md. N.; He, W.; Zarra, T.; Naddeo, V.; Zhao, Y. New Sustainable Approach for the Production of Fe3O4/Graphene Oxide-Activated Persulfate System for Dye Removal in Real Wastewater. *Water* **2020**, *12* (3), No. 733, DOI: 10.3390/w12030733.

(13) Liu, M.; Wen, T.; Wu, X.; Chen, C.; Hu, J.; Li, J.; Wang, X. Synthesis of porous Fe3O4 hollow microspheres/graphene oxide composite for Cr(vi) removal. *Dalton Trans.* **2013**, *42* (41), 14710−14717.

(14) Yang, W.; Zhang, G.; Ni, J.; Wang, Q.; Lin, Z. From signal amplification to restrained background: Magnetic graphene oxide assisted homogeneous electrochemiluminescence aptasensor for highly sensitive detection of okadaic acid. *Sens. Actuators, B* **2021**, *327*, No. 128872.

(15) He, G.; Liu, W.; Sun, X.; Chen, Q.; Wang, X.; Chen, H. Fe3O4@graphene oxide composite: A magnetically separable and efficient catalyst for the reduction of nitroarenes. *Mater. Res. Bull.* **2013**, *48* (5), 1885−1890.

(16) Foroutan, T.; Kabiti, F.; Motamedi, E. Silica Magnetic Graphene Oxide Improves the Effects of Stem Cell-Conditioned Medium on Acute Liver Failure. *ACS Omega* **2021**, *6* (33), 21194−21206.

(17) He, F.; Fan, J.; Ma, D.; Zhang, L.; Leung, C.; Chan, H. L. The attachment of Fe$_3$O$_4$ nanoparticles to graphene oxide by covalent bonding. *Carbon* **2010**, *48* (11), 3139−3144.

(18) Hummers, W. S.; Offeman, R. E. Preparation of Graphitic Oxide. *J. Am. Chem. Soc.* **1958**, *80* (6), 1339.

(19) Yang, X.-R.; Song, X.-D.; Zhu, H.-Y.; Cheng, C.-J.; Yu, H.-R.; Zhang, H.-H. Novel Smart Polymer Brushes Modified Magnetic Graphene Oxide for Highly Efficient Chiral Recognition and Enantioseparation of Tryptophan Enantiomers. *ACS Appl. Bio Mater.* **2018**, *1* (4), 1074−1083.

(20) Liu, X.; Yan, L.; Yin, W.; Zhou, L.; Tian, G.; Shi, J.; Yang, Z.; Xiao, D.; Gu, Z.; Zhao, Y. Magnetic graphene hybrid functionalized by beta-cyclodextrins for fast and efficient removal of organic dyes. *J. Mater. Chem. A* **2014**, *2*, 12296−12303.